HHS Public Access

Author manuscript

J Neural Eng. Author manuscript; available in PMC 2018 June 12.

Published in final edited form as:

J Neural Eng. 2015 October ; 12(5): 056005. doi:10.1088/1741-2560/12/5/056005.

A wireless transmission neural interface system for unconstrained non-human primates

Jose A. Fernandez-Leon[1,2,5,*], **Arun Parajuli**[1,*], **Robert Franklin**[3], **Michael Sorenson**[3], **Daniel J. Felleman**[1], **Bryan J. Hansen**[1,4], **Ming Hu**[1], and **Valentin Dragoi**[1]

[1]Department of Neurobiology and Anatomy, University of Texas–Houston Medical School, Houston, TX 77030, USA

[2]Centre for Computational Neuroscience and Robotics, University of Sussex, Brighton BN1 9QG, United Kingdom

[3]Blackrock Microsystems, Inc. Salt Lake City, UT 84108, USA

[4]Systems Neurobiology Laboratory, The Salk Institute for Biological Sciences, La Jolla, CA 92037, USA

Abstract

Objective—Studying the brain in large animal models in a restrained laboratory rig severely limits our capacity to examine brain circuits in experimental and clinical applications.

Approach—To overcome these limitations, we developed a high-fidelity 96-channel wireless system to record extracellular spikes and local field potentials from neocortex. A removable, external case of the wireless device is attached to a titanium pedestal placed in the animal skull. Broadband neural signals are amplified, multiplexed, and continuously transmitted as TCP/IP data at a sustained rate of 24 Mbps. A Xilinx Spartan 6 FPGA assembles the digital signals into serial data frames for transmission at 20 kHz though an 802.11n wireless data link on a frequency shift key modulated signal at 5.7-5.8 GHz to a receiver up to 10 m away. The system is powered by two CR123A, 3-V batteries for 2 hours of operation.

Main results—We implanted a multi-electrode array in visual area V4 of one anesthetized monkey (*Macaca fascicularis*) and in the dorsolateral prefrontal cortex (dlPFC) of a freely moving monkey (*Macaca mulatta*). The implanted recording arrays were electrically stable and delivered broadband neural data over a year of testing. For the first time, we compared dlPFC neuronal

Address correspondence to: Valentin Dragoi, Department of Neurobiology and Anatomy, University of Texas-Houston Medical School, 6431 Fannin St., Houston, TX 77030, USA, Phone: (713)-500-5710, Fax: (713)-500-0621, valentin.dragoi@uth.tmc.edu.

[5]Current Address: Department of Neuroscience, Baylor College of Medicine, Houston, TX 77030, USA

[*]These authors contributed equally to this work

AUTHOR CONTRIBUTIONS

VD conceived and supervised the project. JAF-L and AP designed the experiments and performed the recordings. JAF-L and AP implemented all the analyses. MS and RF designed and implemented the wireless transmitter/receiver physical devices, and provided technical descriptions. DJF performed the surgery of the implanted multi-electrode arrays and assisted in the initial testing of the wireless system from one anesthetized monkey. BJH participated in the early stages of the project. JAF-L, AP, and VD wrote the manuscript. All authors made comments on the manuscript.

COMPETING FINANCIAL INTERESTS

MS and RF have a financial interest in Blackrock Microsystems. No other author declares competing financial interests.

responses to the same set of stimuli (food reward) in restrained and freely moving conditions. Although we did not find differences in neuronal responses as a function of reward type in the restrained and unrestrained conditions, there were significant differences in correlated activity. This demonstrates that measuring neural responses in freely-moving animals can capture phenomena that are absent in the traditional head-fixed paradigm.

Significance—We implemented a wireless neural interface for multi-electrode recordings in freely moving non-human primates which can potentially move systems neuroscience to a new direction by allowing to record neural signals while animals interact with their environment.

Keywords

freely-moving monkey; wireless; cortex; electrophysiology

INTRODUCTION

The neural underpinnings of complex behavior have been typically investigated in non-human primate models, which offer several key evolutionary advantages over other mammalian species. However, these investigations are currently performed in the laboratory environment under artificial conditions in which animals are totally or partially restrained and tethered to a recording system via a cable that carries electrical signals from electrodes inserted in the brain (e.g., Dragoi et al., 2002, Gutnisky and Dragoi, 2008, Jog et al., 2002, Felsen and Dan, 2005, Lewen et al., 2001). While tremendous advancements in neuroscience have been achieved by using recording devices transmitting data via constraining cabled electronics, it remains unclear whether phenomena observed in laboratory conditions, such as changes in neuronal responses during adaptation, learning, or decision making can be replicated when animals behave in their natural environment. Indeed, the responses of individual neurons in many brain areas are sometimes different in natural environments compared to when they are measured in laboratory conditions. For instance, the responses of neurons in many visual cortical areas are sparser (less dense) and more reliable when natural scenes or movies are presented than when artificial stimuli are being used (Vinje and Gallant, 2000, Froudarakis et al., 2014). These difficulties can be overcome by using a high fidelity wireless technology capable of transmitting broadband signals from large populations of neurons while animals are unrestrained (Borton et al., 2013, Schwarz et al., 2014, Szuts et al., 2011, Wilson et al., 2003, Yin et al., 2013, Yin et al., 2014).

Several wireless recording systems have been developed for a variety of freely moving animal models such as rodents (Rizk et al., 2007, Szuts et al., 2011, Lee et al., 2013), sheep (Rizk et al., 2009), and non-human primate (Borton et al., 2013, Miranda et al., 2010, Ryou and Wilson, 2004, Schwarz et al., 2014, Foster et al., 2014, Foster et al., 2012, Chestek et al., 2011, Chestek et al., 2009) using commercial off the shelf electronics. However, there are still limitations in the development of the wireless technology in terms of trade-offs between power consumption, performance in data transmission, quality of signals, and device size. For instance, despite their low cost, these early systems have a high power consumption, which makes it difficult to run freely behaving experiments for extended periods of time. Comparing implantable systems to external systems, additional limitations include the number of channels that can be placed in multi-electrode array (MEA) devices and the

capacity of transmitting high quality, multiunit signals (Greenwald et al., 2011, Yin et al., 2013, Yin et al., 2014). In particular, one of the main challenges of previous wireless systems has been the development of a cost efficient and reusable wireless transmitting device that sends large amounts of neural signals across time in unconstrained, mobile animals (Schwarz et al., 2014, Borton et al., 2013). Whereas our recording system (based on the Atheros 802.11n chipset running custom firmware) does not offer solutions to all of the limitations of the previous wireless systems, it does represent a tradeoff between consumption power and size of wireless transmitter while improving the signal transmission distance.

Here we report the development of a compact 96-channel neural interface wireless system that meets the requirements to ensure the recording of extracellular spikes and local field potentials (LFPs) from cortical areas in freely-moving non-human primates. Our system allows the wireless transmission of neural signals over longer distances by increasing the power of the wireless transmitter, and using a Multiple-Input Multiple-Output (MIMO) configuration and omnidirectional antennas that are more conducive to common animal environments than other reported systems (further discussed in the next section). We demonstrate the performance of our wireless technology for brain research by acquiring broadband neural recordings from nonhuman primates in visual area V4 and dorsolateral prefrontal cortex (dlPFC). The broadband transmitter was attached to a skull-mounted titanium pedestal that connects to a microelectrode Utah array (Blackrock Microsystems, LLC). The wireless transmitter incorporates several low power custom integrated circuits and includes the benefits of the 802.11n IEEE wireless data link, rather than the existing radio topologies currently used for wireless neural recordings. The acquisition of neural signals was possible through implanted conventional microelectrode Utah arrays implanted in visual cortex and dlPFC – our analyses indicated that the wireless system performs similarly to the corresponding 96-channel wired recording configuration. To illustrate the capacity of our broadband wireless system for unrestrained animal experimentation, we recorded brain signals from dlPFC in macaque monkey, an area that shows decision related activity in complex tasks (Passingham and Wise, 2012). The flexibility of the wireless system for acquiring broadband neural recordings from unrestrained non-human primates recommend our neuro-technology as a new tool that can potentially transform neuroscience by allowing neuronal recordings in experimental naturalistic conditions.

RESULTS

Configuration of a high fidelity signal transmission wireless telemetry

The wireless transmission system consists of three major components (Fig. 1): (*i*) a multi-electrode array (MEA) connected (Fig. 1A-middle and B) to a (*ii*) skull-mounted pedestal (Fig. 1A-left); (*iii*) a removable, wireless CerePlex radio transmitter (Fig. 1A-right and C) that attaches to the pedestal and transmits neural signals to a radio receiver connected to a conventional multichannel recording system. The other end of the wireless data link consists of the CerePlex radio receiver that processes the data stream and transfers the data using the fiber optic data link format used by the Cerebus Neural Signal Processor (Blackrock Microsystems, LLC).

The MEA consists of a Utah Array assembly (Fig. 1B; Platinum: ~0.4 MΩ @ 1 kHz; insulation: Parylene-C; electrode lengths 1.5 mm; electrode pitch 400 μm) implanted in the brain enabling 96-channel recording of extracellular spikes and local field potentials (see Methods and surgical procedures; Supplemental Figure S.1). The skull-mounted transmitter pedestal (Fig. 1A-left) is connected to the MEA via a wire bundle (25 μm Pt/Au lead wires between electrode array and connector; wire bundle length: 20–130 mm length potted with medical-grade silicone elastomer), and it has two stainless steel ground wires. The wireless transmission system that includes the transmitter pedestal was implemented to be carried by a monkey (Fig. 1C). Fig. 1D shows system schematics of the receiving and processing devices.

A challenge for recording neural signals wirelessly during animal movement is to maintain a reliable and high throughput data link with low energy consumption. The transmitter that we implemented (Fig. 1A-right) consists of several low power, custom integrated circuits that digitize the neural signal at 20 kHz and transmit it over an 802.11n wireless data link. Two 3V batteries (battery size CR123A) power the transmitter (detailed technical descriptions of the transmitter are provided in Supplemental Table T.1). The external case of the wireless device and its attached fan are used for heat dissipation. There are insulating layers between the wireless radio and the digitizing head stage that interfaces with the pedestal. This was done to keep the pedestal out of thermal contact with the radio. Internal testing was performed to ensure that the pedestal would not heat up and cause damage to the animal.

The use of the 802.11n wireless protocol for data transmission provides several advantages over existing radio topologies in the neural recording space. First, the radio wireless transmitter sends multiple data streams simultaneously in a dual antenna through 2×2 MIMO configuration. This allows for faster data transfer (a theoretical maximum transfer rate of 270 Mbps) with better signal integrity in obscured environments that could cause multipath problems. Increasing the data rate to 270 Mbps does not change the power consumption. The reduced data rate (relative to the theoretical maximum) used for the experiments discussed in this paper was chosen to match the electrode configuration and data recording system. Second, the transmission range of our wireless system is about one order of magnitude greater than that of the other existing systems (Supplemental Table T.2). Thereby these features enable robust post-hoc analysis of the acquired data. Although not implemented in this version, data encryption (WPA2 and AES) is easily implemented with the 802.11n transmitter ensuring security of the neural transmitted data. This technology represents a significant increase in the maximum net data rate from 54 Mb/s (802.11g) to 150 Mb/s with a channel width of 40 MHz, 802.11n standardized support for multiple-input multiple-output, frame aggregation, and security improvements, among other features. The system can be used either in the 2.4 GHz or 5 GHz frequency bands (IEEE, 2009). In particular, real world bit error rates (BER) in standard lab settings vary greatly due to multipath issues. A comparison of theoretical BER vs signal-noise-ratio across the different varieties of 802.11 (a/b/g/n) radios can be found in Khanduri and Rattan (2013).

A detailed block diagram of the transmitter CerePlex digital wireless system is shown in Fig. 1E. Electrode signals from 96 electrode channels are fed into a custom-designed, amplifier application-specific integrated circuit (ASIC). The ASIC band pass filters each electrode

signal from 0.03 to 7.5 kHz, and then multiplexes the 96 channels from three banks of 32 channels into 3 single channels at 960 kSps. Each channel is converted to a 12-bit digital signal using off the shelf ADC chips (AD7984BRMZ). A Xilinx Spartan 6 FPGA then assembles the digital signals into serial data frames. Each frame includes a sync sequence, status flags, serial data, and packet footer. The serialized data frames are collected by an ARM processor (TI OMAP3503) running a real-time Linux kernel and then passed as TCP/IP data to an Atheros 802.11n chipset running custom firmware. The system described here uses commercially available electronics as opposed to the custom ASIC used in other comparable wireless systems (e.g., (Yin et al., 2014, Borton et al., 2013).

Because of electromagnetic interference, wireless telemetry systems must be designed to avoid signal loss and be designed for high fidelity signal transmission in open, more complex environments. These desired features of a wireless system were the main motivations for the design of our wireless system as explained below. The described circuitry guarantees continuous transmission of TCP/IP data at a sustained rate of 24 Mbps. The Atheros chipset uses a dual band Wi-Fi chip antenna (Johnson Technology 2450AD46A5400E) to transmit the data. The receiver system uses standard 2400 MHz omnidirectional Wi-Fi antennas to receive the transmitted signals. The radio frequency (RF) receiver transmission range (radio power 15 dBn) can be extended from 32 ft by in-line positioning of additional antennae in 6.5 ft increments. The electronic operating environment of the system ranges from 10° to 40°C, 5 to 95% relative humidity (non-condensing) with a sampling frequency of 20 kHz. The receiver uses the exact same topology found in the transmitter (Atheros chipset, ARM processor, and FPGA) to remove the TCP/IP wrapper from the data, and then converts the data into a format compatible with the Cerebus Digital Hub for fiber optic transmission to the Cerebus Neural Signal Processor. In brief, the proposed wireless configuration has the potential to achieve spatial coverage within spatially complex environments with high fidelity signal transmission.

Wireless transmissions are comparable to wired recordings

We assessed the performance of our wireless transmission system by transmitting a well-defined signal generated by the Blackrock Neural Signal Simulator and comparing it to that recorded by our system after receiving it wirelessly. The simulator generates identical signals consisting of both spikes and LFP in all of its 96 channels. Fig. 2A shows the transmitted and received spike trains from an example channel consisting of a burst of 99 spikes with 3 different waveform shapes lasting 1 second, resulting in a firing rate of 99 spikes/second during the burst period. The LFP generated by the simulator is a linear combination of 1, 3, 9, and 20 Hz sine waves and was found to remain almost identical after being transmitted and received by the wireless system (Fig. 2B). We compared the transmitted and received signals and observed almost identical signals (Fig. 2A-B), which highlights the fidelity and uninterrupted collection of broadband neural data. The signal generated by the simulator (i.e. the transmitted signal) was estimated by measuring it with the wired recording setup.

To verify the quality of the spike waveforms recorded with our wireless system, we recorded the simulated signal using both wired and wireless setups and performed cluster analysis of

spike waveforms (w/f 1600 μsec; pre-threshold 300 μsec; A/D Freq. 30 MHz). In particular, the difference between the classified waveforms was small comparing both clusters (i.e., wired and wirelessly transmitted waveforms), reporting an average difference of 1.47 % waveforms per cluster (Fig. 2C). The waveform shapes and resulting principal component clusters from the wired and wireless recordings were also almost identical to each other (difference in waveform amplitude between the two methods range ±5 μV) (Fig. 2D). To compare the signal quality, we applied a well-established spike sorting technique indicating that this similarity is also evident when comparing the main eigenvalues of the principal component analysis (PCA, Fig. 2E) used for clustering the wired signal and wirelessly received waveforms. Next, we examined the fidelity of our wireless system as a function of distance. By using a omnidirectional antenna in the receiver and maintaining a line of sight between the wireless transmitter and the receiver, the transmission quality remained very high (~98% of detected waveforms) over a 10 m distance (Fig. 2F), beyond which the signal started to slowly degrade.

Since the low amplitude analog signals are digitized prior to transmission, no interference issues from external radio frequency sources were detected during tests. Using standard methods, we calculated the random noise in the system by comparing the received raw signal from an individual channel to the average of the 96 nominally identical output channels of the neural signal generator. Similarly, the systematic noise was determined by comparing the average of 96 received signals to the average of 96 output channels of the neural signal generator. The random noise and systematic noise were found to be 2.89 $\mu V_{r.m.s.}$ (r.m.s.: root-mean-squared) and 2.65 $\mu V_{r.m.s.}$ respectively. When added in quadrature (square root of the sum of the squares) the resultant total noise due to the system was 3.93 $\mu V_{r.m.s.}$, which is well below the biological noise inherent in extra-cellular recording(Lopez et al., 2012) (a detailed description of the performance of our wireless system is shown in Supplemental Table T.2; our system had an overall lower noise level ($\mu V_{r.m.s}$) when compared to other systems (see Borton et al., 2013 for comparisons).

Wireless recordings in anesthetized, restrained, and freely-moving conditions

We first tested the quality of the LFP signals acquired using our wireless system by recording LFP responses of visual cortical (area V4) neurons of one anesthetized monkey using drifting oriented gratings (see Methods), and compared the wireless and wired recordings (Fig. 3A). Broadband (1-250 Hz) LFP signals (Fig. 3B) were recorded from 96 channels while moving luminance-contrast grating (6 orientations × 2 directions) stimuli were presented for 200 ms with 50 repetitions in pseudorandom order. By computing the complex Morlet wavelet transform of the LFP signal, we found strong responses to visual stimuli in both low and high frequency bands (Fig. 3C). By examining the mean stimulus-evoked gamma power for each of the 12 stimuli, we found a strong preference for the orientation and direction of the stimuli (Fig. 3D). The quality of the LFP signals and the responses to stimuli obtained by recording with our wireless system was found to be as good as that of the wired system.

We next tested the suitability of our wireless recording system for freely moving non-human primates. We recorded single units and LFPs from 96 electrodes chronically implanted in

dorsolateral prefrontal cortex (dlPFC) in one animal using the wired (Fig. 4A-left) and wireless (Fig. 4A-right) recording techniques (using the same skull-mounted pedestal). Single units were extracted and sorted from the 96-channel uninterrupted raw data (Fig. 4B for both conditions). Across all the recording sessions, we identified single and multi-unit spiking activity (using principal component analysis) from 35.4% (34 out of 96) of the channels (an example is shown in Fig. 4C). For restrained and freely moving conditions, Fig. 4D shows examples of raster plots representing stable single unit activity from 16 electrodes for a period of 5 s – waveforms were found to be very similar for both restrained and unrestrained recording conditions (Fig. 4E). This indicates that our wireless recording system yields single unit data that is comparable to the direct, wired recording system.

To assess the stability of our chronic recordings, we analyzed spike waveforms from electrodes across 37 days (Fig. 4F; a total of 165 single units were detected across 10 sessions). The example in Fig. 4F shows that the spike waveforms of the neurons recorded wirelessly were remarkably stable even after 37 days. Supplemental Figure S.2 shows the probability distribution of impedance values of electrodes. Based on this distribution, we identified good quality single units during one session recorded 12 months after the initial implant surgery. This figure indicates that a high impedance (>0.6 MΩ) was observed in most of the electrodes even after several months since the implant (mean impedance 0.73 ± 0.17 MΩ).

Wireless monitoring of population activity during free exploration

Cortical neurons typically exhibit correlations in their firing on time scales from milliseconds to seconds (Cohen and Kohn, 2011, Smith and Sommer, 2013). We thus measured the cross correlation between pairs of dlPFC neurons recorded from the same or different channels while the monkey was freely moving in its cage. While most pairs (73.7%) showed peaks near zero lag (Fig. 5A-bottom) to indicate synchronized firing, pairs with correlation peaks displaced from the zero lag were observed less often (Fig. 5A-top). We measured the strength of synchronized firing between two neurons using a correlation index defined as the ratio of the mean value in a 40-ms central window around 0 s delay relative to the baseline (mean value around delays of ±1 s) (Szuts et al., 2011). Across all the recorded pairs (Fig. 5B), the correlation index was biased to positive values, possibly due to changes in the visual input as the animal moves in its environment (most correlation values were greater than 1 to indicate that central peaks were found most frequently) or to influences from other brain areas (Niell and Stryker, 2010).

We next examined how the correlation index varies as a function of the distance between the dlPFC neurons (see also (Leopold et al., 2003); correlations were computed regardless of the kinematics or gaze of the animal). We found a peak in the correlation index between dlPFC cell pairs from the same electrode, and a sharp decline in mean correlation index between neurons separated by 400 μm or more (Fig. 5C-inset). Similar results were found when examining spike train correlations as a function of distance (Supplemental Fig. S.3 and Fig. S.4). Nonetheless, correlations remained high when they were measured on different electrodes to indicate that correlated firing extends over large distances during free behavior. Whereas our preliminary tests were not designed to explore possible mechanisms, such

patterns may be caused by stimulus-induced correlations during the viewing of natural scenes or optic flow from the animal's movements, or by long-range cortical networks. Additionally, we found that the variance of the correlation index increases with the distance between electrodes (Fig. 5C).

We have also measured the correlations in LFP power by computing (Fig. 5D) the Pearson correlation of band-limited LFP power between two electrodes as a function of electrode distance (in the 400-4400 μm range). We found that LFP correlations decrease as a function of electrode distance – LFP power correlations for low frequencies (2-12 Hz encompassing delta, theta, and alpha frequencies) decreased slowly with distance, whereas high frequency (12-100 Hz, i.e., beta and gamma frequencies) LFP power correlations decreased more rapidly.

Reward modulation of neuronal activity in restrained and unrestrained conditions

A fundamental drawback of conventional electrophysiological techniques is the necessity of unnatural levels of movement restraint (Gilja et al., 2010). However, it is unknown whether and how this movement restriction impacts cell responses during stimulus encoding. As a preliminary experiment to justify the use of wireless neuronal recordings in freely moving animals, we compared neuronal responses in restrained and freely moving conditions when different food rewards, i.e., preferred and non-preferred food (see Methods), were presented to the animal (this experiment represents an ethologically relevant task associated with foraging, (Glavis-Bloom et al., 2013). This investigation was motivated by evidence that prefrontal cortex is involved in acquiring and maintaining information about stimulus context (Watanabe et al., 2002, Funahashi et al., 1989) and reward expectancy (Hikosaka and Watanabe, 2000, Leon and Shadlen, 1999, Rainer et al., 1999). Indeed, in order to select the best foraging targets (i.e., preferred and non-preferred food sources), an animal must integrate uncertain sensory cues (reward location and timing) with memory of past reward events (Glavis-Bloom et al., 2013), and these features are typically attributed to prefrontal cortex (PFC) (Passingham and Wise, 2012). Although previous studies have measured PFC responses to different types of reward (Ryou and Wilson, 2004), neuronal recordings were performed under highly-restrained conditions (Squire et al., 2013, Wallis, 2007, Wallis and Miller, 2003, Sakurai and Takahashi, 2006).

We examined the changes in dlPFC responses in two conditions: (*i*) head-fixed and movement restrained condition (Fig. 6A-top) and (*ii*) when the animal freely roamed in its cage (Fig. 6A-bottom, see Methods). In both conditions, the animal was first visually exposed for 10 s to food reward (preferred: grape slice, and non-preferred: cucumber slice) provided by the experimenter in pseudo randomly interleaved trials ~20 cm away from the cage (reward presentation; Fig 6A, see Methods). Reward presentation was cued by a specific sound that was identical for both types of reward. In the freely moving condition, the monkey was able to roam through the cage during the entire reward presentation. Behavioral events were recorded with a video camera facing the front of the cage and synchronized to neural events by impulses sent to the recording device. The monkey performed 24 trials per reward type per session (5 restrained and 5 freely moving sessions), and each reward type represented one trial (timeline in Fig. 6B). As expected, the animal

consumed the preferred reward more often than the non-preferred reward (P<0.001, Wilcoxon rank-sum test; Fig. 6C). Overall, in the freely moving condition we were able to observe a variety of behaviors that were unavailable in the restrained condition, such as moving close to the experimenter when the preferred reward was presented, and moving away from the experimenter when the non-preferred reward was presented to the monkey. We quantified the movement of the animal in Fig. 6E by video recording the movements of the monkey in the freely-moving condition, and then tracking the movements of the monkey's head offline by using the transmitter as the reference point (see Methods). Although the animal was allowed to freely move in its cage during reward presentation, we did not observe a significant difference between the extent of movement (Fig. 6D) associated with the preferred and non-preferred reward types during reward presentation (Fig. 6E, P>0.1, Wilcoxon rank-sum test; see Methods).

Reward-dependent changes in neuronal correlations in the unrestrained condition

We further examined neuronal responses to the two types of reward in the restrained and unrestrained conditions (Supplemental Fig. S.5 shows the probability distribution of the average firing rates of neurons). Fig. 7A depicts the firing rate histograms for one example neuron responding to both types of reward (the evoked response lasts for about 1 s; see also refs. 40–42). Surprisingly, we did not find a significant difference between the mean firing rates for the two reward types after stimuli were presented (as the neural response to reward was characterized by a strong onset transient followed by a decrease to baseline firing, we focused the analysis on the first 1000 ms after stimulus presentation). Indeed, the population average firing rates for the two rewards types (Fig. 7B, 1000 ms following stimulus onset) were not significantly different from each other during the restrained (P=0.43; preferred: 1.95±0.25 Hz, non-preferred: 2.05±0.27 Hz; mean±sem, n=86) and freely moving conditions (P=0.62; preferred: 1.86±0.38 Hz, non-preferred: 1.96±0.39 Hz, n=79; Wilcoxon sign-rank test), and similar results were obtained when we extended the size of the window in which spikes were counted for the entire 10 s interval when stimulus was presented. This indicates that the firing rates of the dlPFC neurons remained unchanged during reward presentation, irrespective of reward type and regardless of whether the monkey was restrained (1.99±0.24 Hz) or unrestrained (1.91±0.37 Hz, P>0.3, Wilcoxon rank-sum test).

Since we did not find any difference in neuronal responses as a function of reward type in the restrained and unrestrained conditions, we reasoned that possible differences could be detected in the population activity. Therefore, we measured pair-wise correlations between the responses of cells recorded from different electrodes for the first 1000 ms following stimulus presentation in the two behavioral conditions. Fig. 7C shows the average Pearson correlation values associated with the two reward types as a function of expanding window size starting from the time when the reward was first presented. Surprisingly, when the animal was freely moving, correlations dropped significantly when reward was non-preferred. Indeed, the mean correlation coefficient associated with the two types of reward were significantly different from each (Fig. 7D-right; 0.8 s: P=0.038; 0.9 s: P=0.008; 1.0 s: P=0.017; 1.1 s: P=0.029, Wilcoxon sign-rank test). However, when the monkey was restrained neuronal correlations associated with the preferred and non-preferred rewards were not statistically different (Fig. 7D-left; P>0.1, Wilcoxon sign-rank test). Importantly, in

the freely moving condition, the difference in correlations between the responses associated with the two types of reward disappeared when correlations were computed before reward was presented (window size: 1000 ms; P=0.86; Wilcoxon rank sum test; Supplemental Figure S.6). Furthermore, when trials were shuffled for each of the preferred and non-preferred reward conditions correlation coefficients became almost zero (Fig. 7C, dashed lines). That is, despite the fact that preferred and non-preferred reward evoked similar firing rates irrespective of whether the animal is restrained or unrestrained, significant changes in neuronal correlations reflected the animal's reward preference only in the unrestrained condition. These changes in correlations between neuronal responses to preferred and non-preferred reward are likely to reflect the animal's subsequent intention to access the reward and/or interact with the experimenter, which can both differ depending on reward type. Overall, these results indicate that our wireless recording system provides the unprecedented opportunity to examine neuronal populations during free movement and hence uncover new reward encoding strategies that can only be revealed in unrestrained animals.

DISCUSSION

We designed and tested a wireless transmission, neural interface system enabling high quality broadband neural recordings of neuronal data with performance comparable to conventional wired recording systems. By illustrating examples of unrestrained and restrained non-human primate wireless recordings in visual and prefrontal cortex, we demonstrate the potential of our wireless transmission system to collect single units, LFPs, and population activity in freely moving conditions. The main advantage with this new device is the larger transmission range and possibly improved fidelity in data transmission in more complex environments.

From an engineering perspective, the system described here has efficient telemetry and performance, which enables adaptable recordings from populations of neurons in more naturalistic scenarios. The system is based on the 802.11n wireless data link standard that is more robust in signal transmission (i.e. no interference from multipath signals generally caused by presence of metal in the vicinity of the setup) than previous existing radio topologies used for neural recordings. Our wireless system represents a platform that can be used in the very near future to investigate neural processes in multiple areas of the non-human primate brain in free moving conditions while animals explore their naturalistic environment. Having an external replaceable power source (battery) represents an advantage of our system in comparison to other implantable systems as our system allows an easy battery replacement after they are fully discharged. To exemplify, the system recently reported by (Yin et al., 2014)) was designed with a goal of ultra-low power consumption in order to facilitate a fully implantable wireless system, including a battery and charging circuitry. In the externally mounted version, the charging circuitry is replaced by a larger battery that allows for long data recording sessions. However, the lower power has a direct detrimental effect on the practical range of the wireless signal. The system described in (Yin et al., 2014) uses directional antennas in a SIMO configuration to provide a practical range of 1-2 m with line of site and requires an environment that reduces multipath issues (using specially built plastic cages and removing metal from the animal environment). Our system, however, increases the power which also improves the range of the wireless signal up to 10

m to the receiver. It also uses a MIMO configuration and omnidirectional antennas that are conducive to common animal environments. These features of our system enable us to design better experiments where monkey will be free to move unrestrained in a larger and more natural environment. The telemetry being omnidirectional, only one antenna can be used to cover a large space (a sphere of radius around 10 m). As our system is tolerant to multipath signal transmission, and quality of transmission is not affected by presence of metals in the vicinity of the experimental setup. This allows us to employ most commonly used metal cages for the experiment as for the reported experiments involving freely moving monkey. The digitizing front end of the system used by (Yin et al., 2014)) was designed with a lower power budget, at a cost of increase in noise in its range of transmission (i.e. ~2 m) as shown in Table T.2 compared to the system discussed here. In order to improve our system features, a reduction in power consumption will be considered as the next phase in our system design (see Supplemental Table T.2 for power consumption comparisons). This technical improvement is currently under development (Blackrock Microsystems) with a new second generation wireless system that leverages the greater range offered by the system described here, but at lower power consumption. This improvement will further enhance the utility of our current setup with recordings extended in time.

We illustrate the benefit of performing neural recordings in freely moving conditions by focusing on reward encoding in prefrontal cortex. Until now, technical limitations have prevented detailed comparisons between neuronal responses and coding strategies in restrained and unrestrained conditions. Using an unconstrained non-human primate model, our broadband wireless system enabled us to study reward coding during freely moving conditions in a natural relevant foraging task. Despite the fact that neuronal responses to preferred and non-preferred reward do not differ, we found that neuronal spike-count correlations are significantly lower for non-preferred reward, but only when the monkey is unrestrained. This effect likely reflects the animal’s subsequent intention to directly access the reward and possibly interact with the experimenter. Clearly, these different reward encoding strategies between the restrained and unrestrained conditions could have only been revealed by using a wireless system recording neural signals while animals are freely moving in their environment. In addition, commensurate wireless eye tracking for primate is still needed to fully understand the described natural behavior (Shepherd and Platt, 2006, Kano and Tomonaga, 2013).

We have validated a robust system that will become commercially available, which allows high-yield reliable broadband transmission of neural signals from freely moving non-human primates. Overall, the results presented here demonstrate that our wireless recording system provides a flexible platform to examine neuronal responses underlying natural behavior in non-human primate models, and subsequently allow neuro-prosthetic interventions requiring free moving conditions.

METHODS

Descriptions on methods and any associated references are available in the online version of the paper.

ONLINE METHODS

Surgical procedures

All surgeries involving the insertion of the Blackrock Microsystem 100-channel chronic (Utah) array (Blackrock, 2009) into area V4 and dlPFC were performed in accordance with protocols approved by the Institutional Animal Care and Use Committees at UT-Houston Medical School. The multi-electrode array (MEA) was implanted in dlPFC according to MRI and stereotaxic specifications (Paxinos et al., 2000, Saleem and Logothetis, 2007) (Supplemental Figure S.1). MEA is 4.4 mm by 4.2 mm containing 100 electrodes (0.8 mm length) with 400 μm equidistant spacing between electrode sites. During the surgical procedure, the array was enclosed within the craniotomy and attached under the skin to an external connector pedestal (~16.5 mm height, ~9 mm diameter). The titanium pedestal that connects to a microelectrode Utah array (multielectrode array, MEA) was affixed to the skull with screws and contains the connections to the recording equipment. The MEA was biologically inert and can function implanted in the cortex for two or more years.

MRI acquisition

Brain images of the animal were obtained using a high-definition platform GE SignaHDxt 3.0T MR (General Electrics, Milwaukee, WI, USA) scanner at the MD Anderson Cancer Center using high-density coils with the head positioned in the center of the coils. Gradient specifications of the machine are: amplitude 50 mT/m, slew rate 150 T/m/s; magnet FOV: 48×48×48 cm. The animal was anesthetized with a mixture (4: 1, v/v) of ketamine (ketamine hydrochloride, 10–20 mg/kg i.m.) and xylazine (0.2–0.4 mg/kg i.m.). The animal was placed in a nonferrous stereotaxic head holder. His head was aligned in the scanner using the laser landmark alignment system. We ensured that the planes of the MR unit were parallel to those of the stereotaxic instrument. Duration of the scan was approximately 20–30 min. The animal received 5–8 scans.

Anesthetized monkey preparation

General animal preparation and experimental procedures were carried out using methods described previously (Xiao et al., 2003, Wang et al., 2007, Lim et al., 2009). All procedures were consistent with the guidelines of the Society for Neuroscience for the use of laboratory animals and approved by the Animal Welfare Committee of University of Texas at Houston. One long-tailed macaque monkey (*Macaca fascicularis*) was prepared for semichronic recording by sterile implantation of a 96-channel microelectrode array into V4. The animal was anesthetized with Ketamine (25 mg/kg) and pre-medicated with atropine (0.5 mg/kg, I.M.), intubated and catheterized and then deeply anesthetized using isoflurane gas anesthesia (1-2% in oxygen). A ~10×15 mm craniotomy, approximately 18 mm anterior to the external occipital protuberance, was performed using a dental drill. The prelunate gyrus, lunate sulcus, and dorsal tip of the inferior occipital sulcus were then visualized through the closed dura to ensure array placement into parafoveal V4. The 96-channel Utah microelectrode array was carefully positioned immediately over the cortical region of interest. Following implantation, a sheet of artificial dura (Gortex, Gore Industries) was placed over the array and under the original dura. The dura will then be sutured closed and a second sheet of artificial dura was placed over the dura. Semi-chronic recording sessions

began by induction with ketamine and atropine pretreatment. The monkey was then catheterized, intubated, EKG electrodes are placed on the extremities, and then installed in the stereotaxic headholder. Each recording session lasted a total of 12-24 hours. Anesthesia and paralysis were maintained by a constant intravenous infusion (6-12 μg/kg/hr. Sufentanil and 0.01 mg/kg/hr. Vecuronium bromide and dexamethasone (0.1 mg/kg/hr.) in Lactated Ringer's with 5% dextrose at a rate of 10 ml/kg/hr. The eyes were brought into convergence and focused on the screen of a Trinitron monitor by custom-fit contact lenses and a prism. The whole screen (19°×14°) covered the visual field of the recorded portions of V4 (2°–7° along the vertical meridian).

Stimuli

Visual stimuli were used to test the wireless system in both anesthetized and awake states (wired and wireless recordings), and were generated using custom software implemented using the Visage visual stimulation environment (Cambridge Research Systems) and presented on a Trinitron cathode ray tube monitor. Stimuli consisted of 12 luminance-contrast oriented (6 orientations × 2 directions) gratings of 2 cycles/degree spatial frequency that were moved at 2 cycles/second perpendicularly to the long axis. The stimuli had average luminance of 14 cd/m^2 and were presented for 200 ms each on the Trinitron monitor with a background luminance of 14 cd/m^2. Stimulus luminance was calibrated using a J17 LumaColor meter with a J1803 luminance head (Tektronix, Beaverton, OR, USA).

Spike sorting and LFP data processing

Spiking data were run through an offline-sorting program (Plexon, Dallas, TX, USA) and spikes were manually sorted into single-unit channels based on several parameters, including principal components, the peak and valley timing, voltage, and energy. The unfiltered LFP recording was first treated to remove line noise at multiples of 60 Hz by using Chebyshev type II notch filters. To visualize various frequency components (scales) of the LFP signal as a function of time, we calculated the Scalograms using continuous complex Morlet wavelet transform ('cwt' function of Matlab). To compute LFP power in gamma band, we first applied a band pass Chebyshev type II filter to the signal and then squared it.

Behavioral experiments

All experiments (restrained and unrestrained conditions) were performed in accordance with protocols approved by National Institutes of Health's Guide for the Care and Use of Laboratory Animals (ILAR, 2011). One male rhesus monkey (*Macaca mulatta*) was trained under restrained and unrestrained movement conditions. Restrained: the monkey was head-fixed and movement restrained in a polycarbonate primate chair (Crist instruments Co. Inc.); unrestrained: the animal performed free roaming in a four-panel cage (78.500"H × 28.000"D × 54.125"W). The movements of the monkey in the cage for the freely-moving condition were video recorded. Each behavioral event indicated as 'reward presentation' and 'reward access' in Fig. 6A-B was recorded as a manually triggered pulse originated by the experimenter. The synchronization of the set of pulses to the spike recording was considered for the analyses reported in this work. The movements of the monkey's head during the experiment were tracked from the recorded video using the transmitter as the reference point.

Reward experiments

The monkey was exposed to preferred (a half grape piece) and non-preferred reward (a quarter of cucumber slice). The experimenter presented the reward to the monkey (RP, cued by a brief sound) for 10 s from a distance of 20±2 cm, within an area of 5×5 cm in front of the cage; the onset of reward presentation triggered a pulse to the recording device. After reward presentation, the experimenter approached the monkey for 3 s in which the animal was allowed to access and grab the reward (one trial consisted of one reward presentation). The monkey performed 24 trials per reward type within one hour in each recording session (we collected 5 restrained and 5 freely moving sessions). In the unrestrained experiments, the monkey was able to roam within its cage without any restriction. Its behavior was recorded with a video camera facing the front of the cage. The distance between the animal and the receiver varied from 2 to 4 m. We recorded neuronal activity wirelessly from cells in dorsolateral prefrontal cortex; 165 isolated single units were recorded in total. Recordings from dlPFC neural populations during free movement were compared to those in the movement-restrained condition (see main text).

Data analysis and interpretation

All analyses of the data were performed using custom software written for MatLab (MathWorks, Natick, MA, USA).

Supplementary Material

Refer to Web version on PubMed Central for supplementary material.

Acknowledgments

We thank Tony Wright for advice with behavioral experiments. Charles Beaman and Ariana Andrei for useful comments on an earlier version of this manuscript. This work was supported by the NIH Director's Pioneer Award (VD) number 5-DP1-MH099905.

References

BLACKROCK. Blackrock Microsystems Array Surgical Implant Procedure Training Manual, Rev 5.0. 2009

BORTON DA, YIN M, ACEROS J, NURMIKKO A. An implantable wireless neural interface for recording cortical circuit dynamics in moving primates. J Neural Eng. 2013; 10:026010. [PubMed: 23428937]

CHAE MS, YANG Z, YUCE MR, HOANG L, LIU W. A 128-channel 6 mW wireless neural recording IC with spike feature extraction and UWB transmitter. IEEE Trans Neural Syst Rehabil Eng. 2009; 17:312–21. [PubMed: 19435684]

CHESTEK CA, GILJA V, NUYUJUKIAN P, FOSTER JD, FAN JM, KAUFMAN MT, CHURCHLAND MM, RIVERA-ALVIDREZ Z, CUNNINGHAM JP, RYU SI, SHENOY KV. Long-term stability of neural prosthetic control signals from silicon cortical arrays in rhesus macaque motor cortex. J Neural Eng. 2011; 8:045005. [PubMed: 21775782]

CHESTEK CA, GILJA V, NUYUJUKIAN P, KIER R, SOLZBACHER F, RYU SI, HARRISON RA, SHENOY KV. HermesC: Low-power wireless neural recording system for freely moving primates. IEEE TNSRE special issue on wireless neurotechnology. 2009; 17:330–338.

COHEN MR, KOHN A. Measuring and interpreting neuronal correlations. Nat Neurosci. 2011; 14:811–9. [PubMed: 21709677]

DRAGOI V, SHARMA J, MILLER EK, SUR M. Dynamics of neuronal sensitivity in visual cortex and local feature discrimination. Nat Neurosci. 2002; 5:883–91. [PubMed: 12161755]

FELSEN G, DAN Y. A natural approach to studying vision. Nat Neurosci. 2005; 8:1643–6. [PubMed: 16306891]

FOSTER J, NUYUJUKIAN P, FREIFELD O, GAO H, WALKER R, RYU S, MENG T, MURMANN B, BLACK M, SHENOY KV. A freely-moving monkey treadmill model. Journal of Neural Engineering. 2014; 11

FOSTER JD, NUYUJUKIAN P, FREIFELD O, RYU SI, BLACK MJ, SHENOY KV. A framework for relating neural activity to freely moving behavior. Conf Proc IEEE Eng Med Biol Soc. 2012; 2012:2736–9. [PubMed: 23366491]

FROUDARAKIS E, BERENS P, ECKER AS, COTTON RJ, SINZ FH, YATSENKO D, SAGGAU P, BETHGE M, TOLIAS AS. Population code in mouse V1 facilitates readout of natural scenes through increased sparseness. Nat Neurosci. 2014; 17:851–7. [PubMed: 24747577]

FUNAHASHI S, BRUCE CJ, GOLDMAN-RAKIC PS. Mnemonic coding of visual space in the monkey's dorsolateral prefrontal cortex. J Neurophysiol. 1989; 61:331–49. [PubMed: 2918358]

GILJA V, CHESTEK CA, NUYUJUKIAN P, FOSTER J, SHENOY KV. Autonomous head-mounted electrophysiology systems for freely behaving primates. Curr Opin Neurobiol. 2010; 20:676–86. [PubMed: 20655733]

GLAVIS-BLOOM C, ALVARADO MC, BACHEVALIER J. Neonatal hippocampal damage impairs specific food/place associations in adult macaques. Behav Neurosci. 2013; 127:9–22. [PubMed: 23398438]

GREENWALD E, MOLLAZADEH M, HU C, WEI T, CULURCIELLO E, THAKOR V. A VLSI Neural Monitoring System With Ultra-Wideband Telemetry for Awake Behaving Subjects. IEEE Trans Biomed Circuits Syst. 2011; 5:112–9. [PubMed: 23851199]

GUTNISKY DA, DRAGOI V. Adaptive coding of visual information in neural populations. Nature. 2008; 452:220–4. [PubMed: 18337822]

HARRISON RR, KIER RJ, CHESTEK CA, GILJA V, NUYUJUKIAN P, RYU S, GREGER B, SOLZBACHER F, SHENOY KV. Wireless neural recording with single low-power integrated circuit. IEEE Trans Neural Syst Rehabil Eng. 2009; 17:322–9. [PubMed: 19497825]

HIKOSAKA K, WATANABE M. Delay activity of orbital and lateral prefrontal neurons of the monkey varying with different rewards. Cereb Cortex. 2000; 10:263–71. [PubMed: 10731221]

IEEE. IEEE 802.11n-2009-Amendment 5: Enhancements for Higher Throughput. 2009

ILAR. Guide for the Care and Use of Laboratory Animals. Washington, DC: 2011.

JOG MS, CONNOLLY CI, KUBOTA Y, IYENGAR DR, GARRIDO L, HARLAN R, GRAYBIEL AM. Tetrode technology: advances in implantable hardware, neuroimaging, and data analysis techniques. J Neurosci Methods. 2002; 117:141–52. [PubMed: 12100979]

KANO F, TOMONAGA M. Head-mounted eye tracking of a chimpanzee under naturalistic conditions. PLoS One. 2013; 8:e59785. [PubMed: 23544099]

KHANDURI R, RATTAN S. Performance comparison analysis between IEEE 802.11a/b/g/n standards. International Journal of Computer Applications. 2013; 78:1–20.

LEE SB, YIN M, MANNS JR, GHOVANLOO M. A wideband dual-antenna receiver for wireless recording from animals behaving in large arenas. IEEE Trans Biomed Eng. 2013; 60:1993–2004. [PubMed: 23428612]

LEON MI, SHADLEN MN. Effect of expected reward magnitude on the response of neurons in the dorsolateral prefrontal cortex of the macaque. Neuron. 1999; 24:415–25. [PubMed: 10571234]

LEOPOLD D, MURAYAMA Y, LOGOTHETIS N. Very Slow Activity Fluctuations in Monkey Visual Cortex: Implications for Functional Brain Imaging. Cereb Cortex. 2003; 13:422–433. [PubMed: 12631571]

LEWEN GD, BIALEK W, DE RUYTER VAN STEVENINCK RR. Neural coding of naturalistic motion stimuli. Network. 2001; 12:317–29. [PubMed: 11563532]

LIM H, WANG Y, XIAO Y, HU M, FELLEMAN DJ. Organization of hue selectivity in macaque V2 thin stripes. J Neurophysiol. 2009; 102:2603–15. [PubMed: 19571184]

LOPEZ CM, WELKENHUYSEN M, MUSA S, EBERLE W, BARTIC C, PUERS R, GIELEN G. Towards a noise prediction model for in vivo neural recording. Conf Proc IEEE Eng Med Biol Soc. 2012; 2012:759–62. [PubMed: 23366003]

MIRANDA H, GILJA V, CHESTEK CA, SHENOY KV, MENG TH. HermesD: A High-Rate Long-Range Wireless Transmission System for Simultaneous Multichannel Neural Recording Applications. IEEE Trans Biomed Circuits Syst. 2010; 4:181–91. [PubMed: 23853342]

NIELL CM, STRYKER MP. Modulation of visual responses by behavioral state in mouse visual cortex. Neuron. 2010; 65:472–9. [PubMed: 20188652]

PASSINGHAM, RE., WISE, SP. The Neurobiology of the Prefrontal Cortex: Anatomy, Evolution, and the Origin of Insight. Oxford: Oxford University Press; 2012.

PAXINOS, G., HUANG, XF., TOGA, AW. The Rhesus monkey brain in stereotaxic coordinates. California: Academic Press; 2000.

RAINER G, RAO SC, MILLER EK. Prospective coding for objects in primate prefrontal cortex. J Neurosci. 1999; 19:5493–505. [PubMed: 10377358]

RIZK M, BOSSETTI CA, JOCHUM TA, CALLENDER SH, NICOLELIS MA, TURNER DA, WOLF PD. A fully implantable 96-channel neural data acquisition system. J Neural Eng. 2009; 6:026002. [PubMed: 19255459]

RIZK M, OBEID I, CALLENDER SH, WOLF PD. A single-chip signal processing and telemetry engine for an implantable 96-channel neural data acquisition system. J Neural Eng. 2007; 4:309–21. [PubMed: 17873433]

RYOU JW, WILSON FA. Making your next move: dosolateral prefrontal cortex and planning a sequence of actions in freely moving monkeys. Cognitive, Affective, & Behavioral Neuroscience. 2004; 4:430–443.

SAKURAI Y, TAKAHASHI S. Dynamic synchrony of firing in the monkey prefrontal cortex during working-memory tasks. J Neurosci. 2006; 26:10141–53. [PubMed: 17021170]

SALEEM, K., LOGOTHETIS, NK. A combined MRI and histology atlas of the Rhesus monkey brain in stereotaxic coordinates. London, UK: Elsevier; 2007.

SCHWARZ D, LEBEDEV M, HANSON T, DIMITROV D, LEHEW G, MELOY J, RAJANGAM S, SUBRAMANIAN V, IFFT P, LI Z, AL E. Chronic, wireless recordings of large-scale brain activity in freely moving rhesus monkeys. Nature methods. 2014; 11:670–676. [PubMed: 24776634]

SHEPHERD S, PLATT M. Noninvasive telemetric gaze tracking in freely-moving socially-housed prosimian primates. Methods. 2006; 38:185–194. [PubMed: 16431130]

SMITH MA, SOMMER MA. Spatial and temporal scales of neuronal correlation in visual area V4. J Neurosci. 2013; 33:5422–32. [PubMed: 23516307]

SQUIRE RF, NOUDOOST B, SCHAFER RJ, MOORE T. Prefrontal contributions to visual selective attention. Annu Rev Neurosci. 2013; 36:451–66. [PubMed: 23841841]

SZUTS TA, FADEYEV V, KACHIGUINE S, SHER A, GRIVICH MV, AGROCHAO M, HOTTOWY P, DABROWSKI W, LUBENOV EV, SIAPAS AG, UCHIDA N, LITKE AM, MEISTER M. A wireless multi-channel neural amplifier for freely moving animals. Nat Neurosci. 2011; 14:263–9. [PubMed: 21240274]

VINJE WE, GALLANT JL. Sparse coding and decorrelation in primary visual cortex during natural vision. Science. 2000; 287:1273–6. [PubMed: 10678835]

WALLIS JD. Neuronal mechanisms in prefrontal cortex underlying adaptive choice behavior. Ann N Y Acad Sci. 2007; 1121:447–60. [PubMed: 17846158]

WALLIS JD, MILLER EK. Neuronal activity in primate dorsolateral and orbital prefrontal cortex during performance of a reward preference task. Eur J Neurosci. 2003; 18:2069–81. [PubMed: 14622240]

WANG Y, XIAO Y, FELLEMAN DJ. V2 thin stripes contain spatially organized representations of achromatic luminance change. Cereb Cortex. 2007; 17:116–29. [PubMed: 16467565]

WATANABE M, HIKOSAKA K, SAKAGAMI M, SHIRAKAWA S. Coding and monitoring of motivational context in the primate prefrontal cortex. J Neurosci. 2002; 22:2391–400. [PubMed: 11896178]

WILSON FA, MA YY, GREENBERG PA, RYOU JW, KIM BH. A microelectrode drive for long term recording of neuron in freely moving and chaired monkeys. Journal of Neuroscience Methods. 2003:49–61.

XIAO Y, WANG Y, FELLEMAN DJ. A spatially organized representation of colour in macaque cortical area V2. Nature. 2003; 421:535–9. [PubMed: 12556893]

YIN M, BORTON DA, KOMAR J, AGHA N, LU Y, LI H, LAURENS J, LANG Y, LI Q, BULL C, LARSON L, ROSLER D, BEZARD E, COURTINE G, NURMIKKO AV. Wireless neurosensor for full-spectrum electrophysiology recordings during free behavior. Neuron. 2014; 84:1170–82. [PubMed: 25482026]

YIN M, LI H, BULL C, BORTON DA, ACEROS J, LARSON L, NURMIKKO AV. An externally head-mounted wireless neural recording device for laboratory animal research and possible human clinical use. Conf Proc IEEE Eng Med Biol Soc. 2013; 2013:3109–14. [PubMed: 24110386]

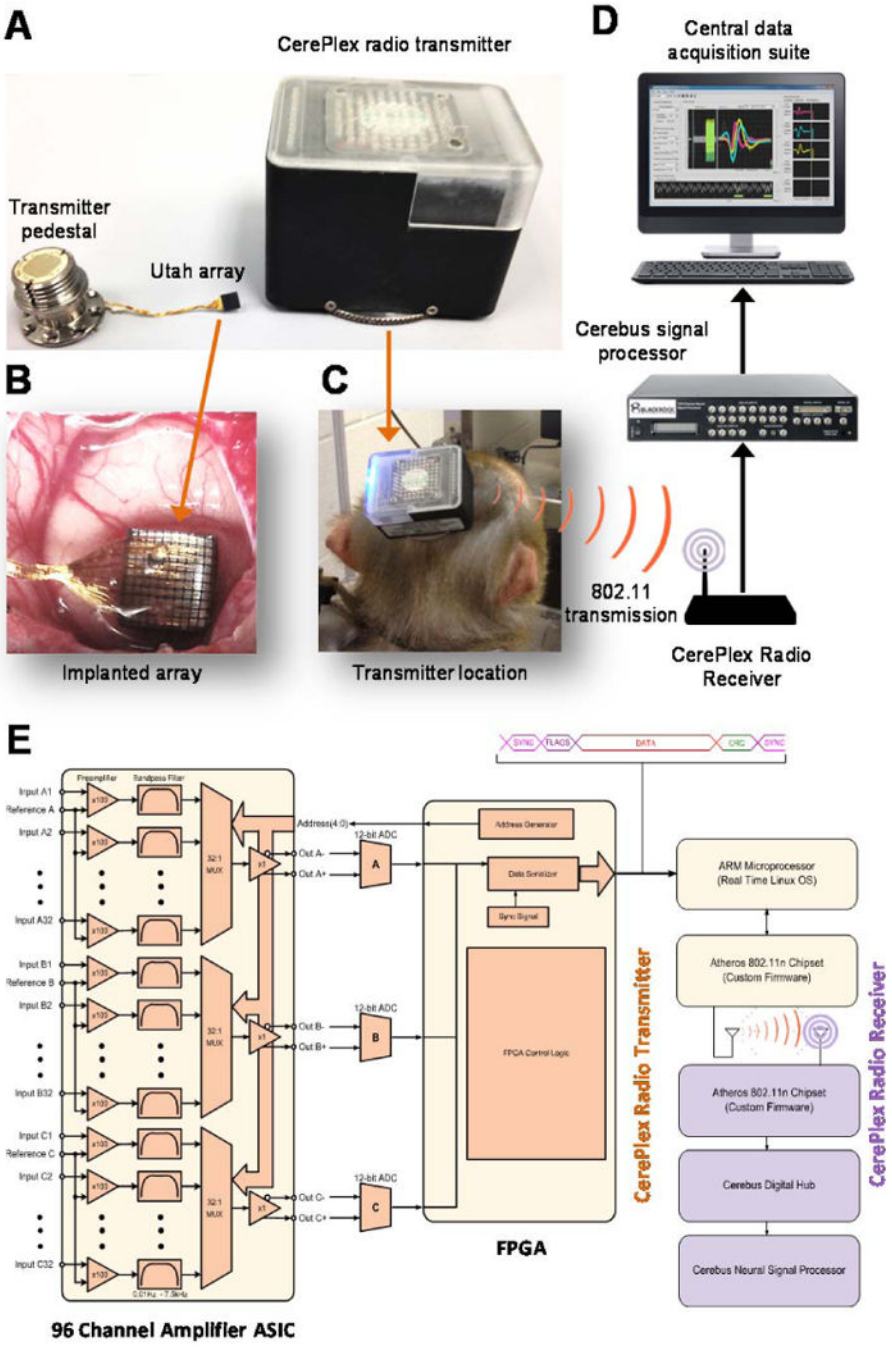

Figure 1.

Configuration of a high-fidelity signal transmission wireless telemetry. (A) A multi electrode array (middle) is connected to a skull mounted pedestal (left). A removable wireless CerePlex radio transmitter (right) attaches to the pedestal and transmits neural signals to a radio receiver connected to a conventional multichannel recording system. (B) Utah array assembly. (C) The wireless transmission system that includes the transmitter pedestal was implemented to be carried by a monkey. (D) Schematics of the data acquisition system. (E) A detailed block diagram of the transmitter CerePlex digital wireless system.

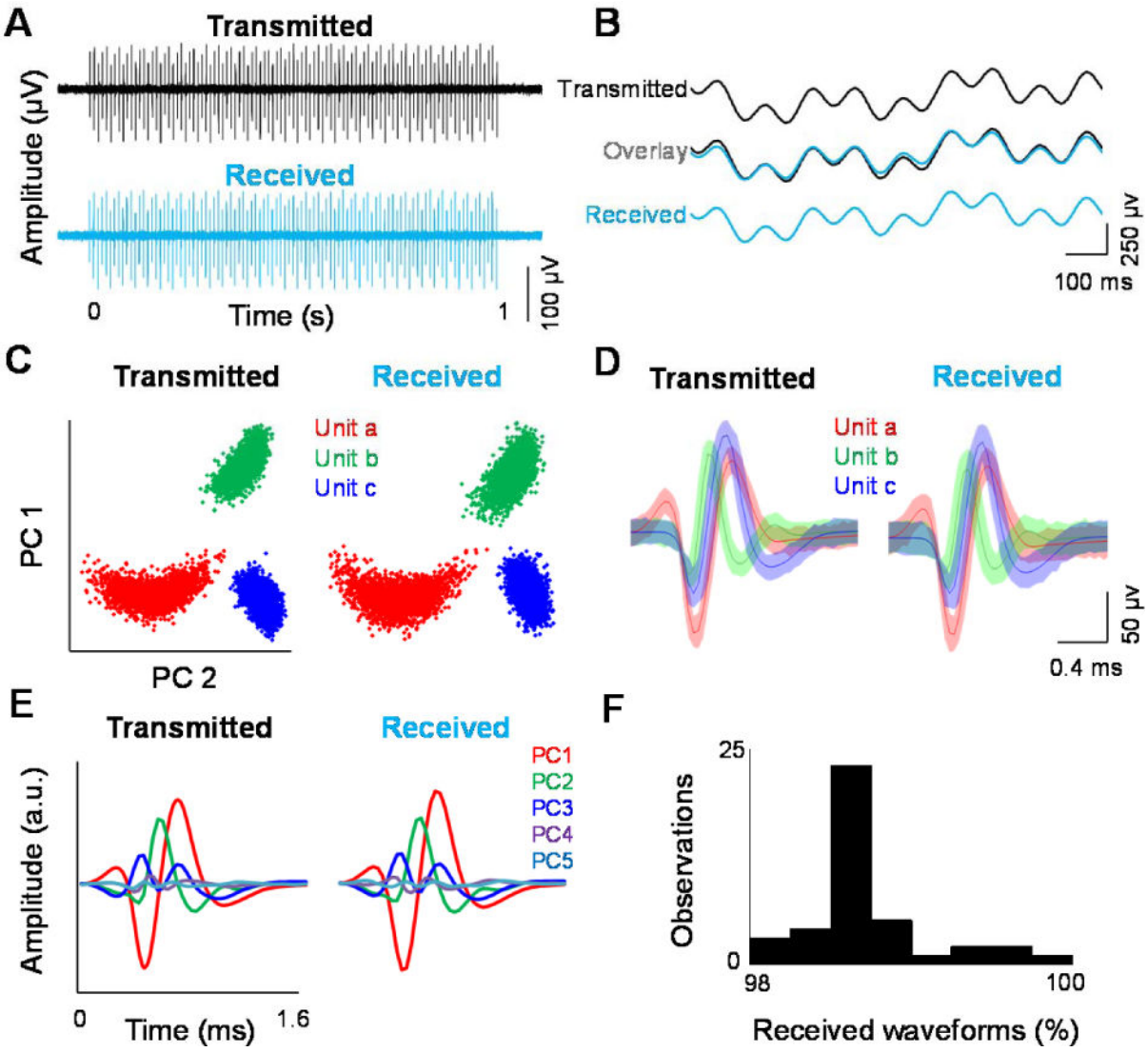

Figure 2.

Wireless transmissions are comparable to wired recordings. Performance of the data transmission system based on a Blackrock neural signal simulator and compares it to that recorded by our system after receiving it wirelessly. (A) Transmitted and received spike trains from an example channel. (B) Example of the transmitted and received local field potentials generated by the simulator. (C) Example of the recorded simulated signal using both wired and wireless setups and performed cluster analysis of spike waveforms. (D) The waveform shapes and (E) resulting principal component clusters from the transmitted and received signals. (F) Performance of the transmission based on the percentage of detected wave forms at 10 m distance between the receiver and transmitter.

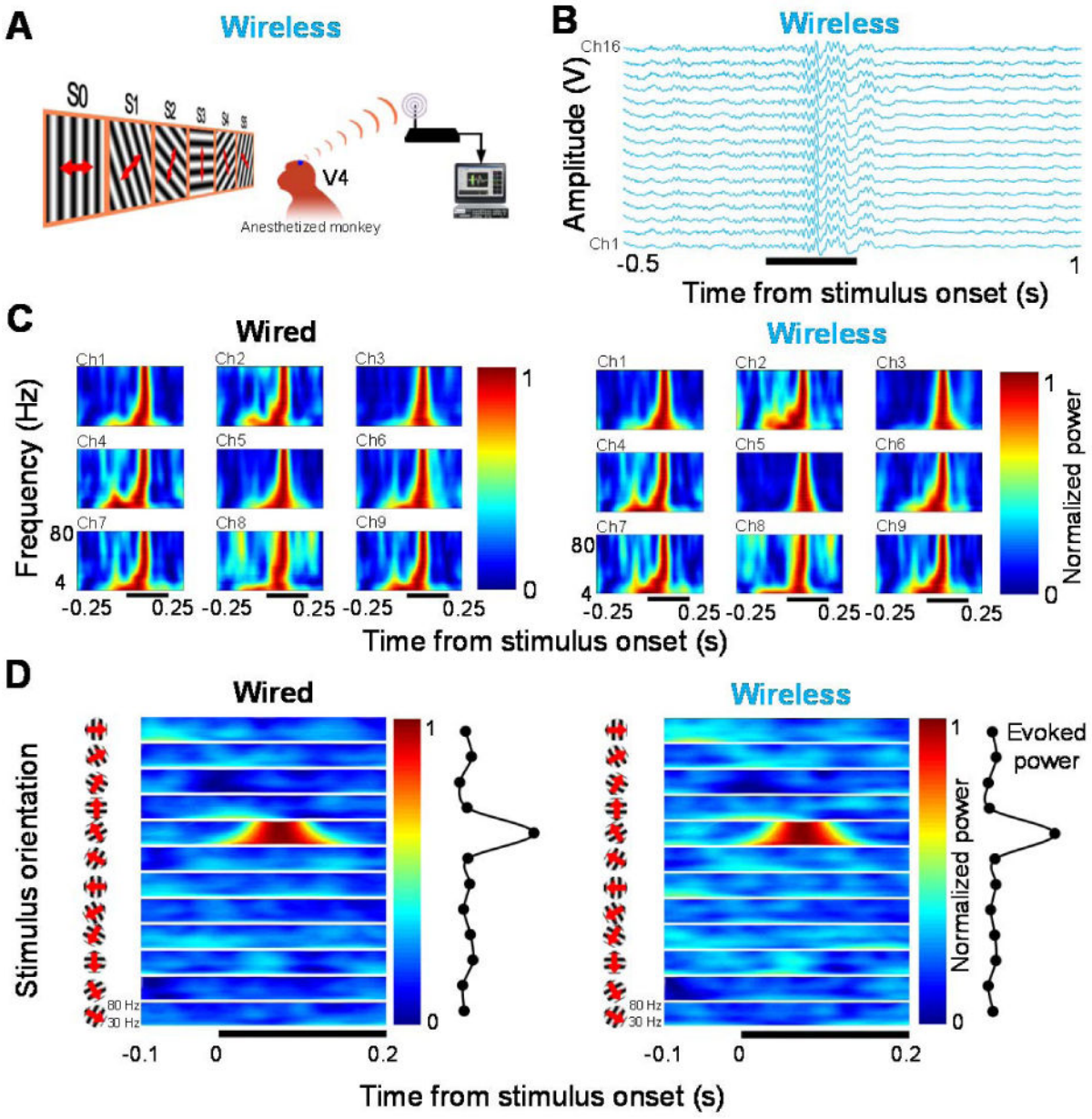

Figure 3.

Wireless recordings in anesthetized condition. Quality of the LFP signals acquired using our wireless system by recording LFP responses of visual cortical (area V4) neurons of one anesthetized monkey, and compared the wireless and wired recording. (A) Schematics of the drifting oriented gratings used as stimuli (see methods). (B) Broadband (1–250 Hz) LFP signals were recorded from 96 channels while moving luminance-contrast grating. (C) For both wired and wireless recordings, results showed strong responses to visual stimuli in both low- and high-frequency bands, and (D) a strong preference for the orientation and direction of the stimuli (see main text).

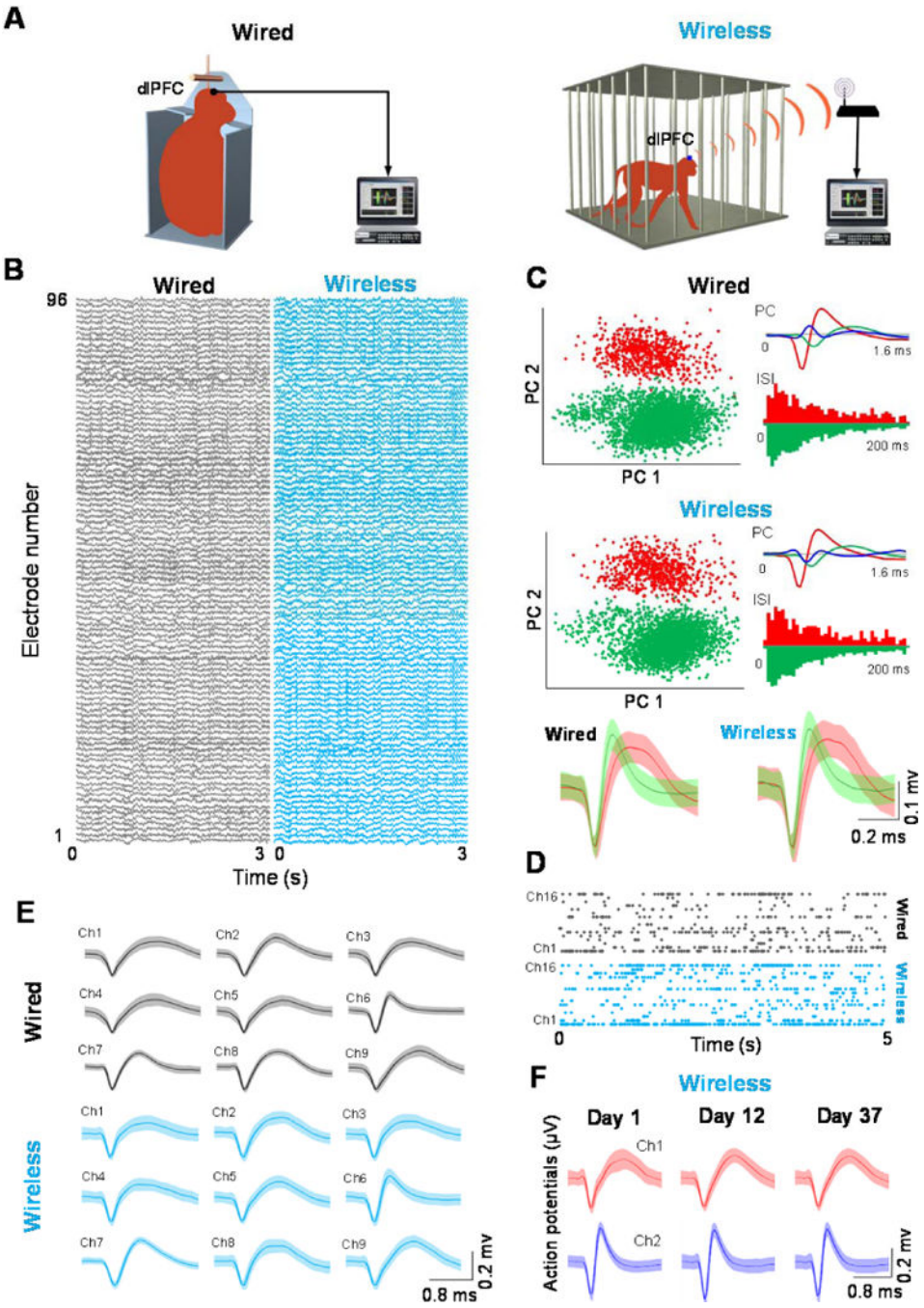

Figure 4.

Wireless recordings in restrained (wired) and freely moving (wireless) conditions. Tests of our recording system for freely moving, non-human primates by recording single units and LFPs from 96 electrodes chronically implanted in the dlPFC in one animal. (A) The wired (left) and wireless (right) recording conditions. (B) Single units were extracted and sorted from the 96-channel uninterrupted raw data for both conditions. (C) Example of the identified single- and multi-unit spiking activity (using principal component analysis). (D) Examples of raster plots representing stable single-unit activity from 16 electrodes for a

period of 5 s. (E) Waveforms were found to be very similar for both restrained and unrestrained recording conditions. (F) Plot showing that the spike waveforms of the neurons recorded wirelessly were remarkably stable even after 37 days.

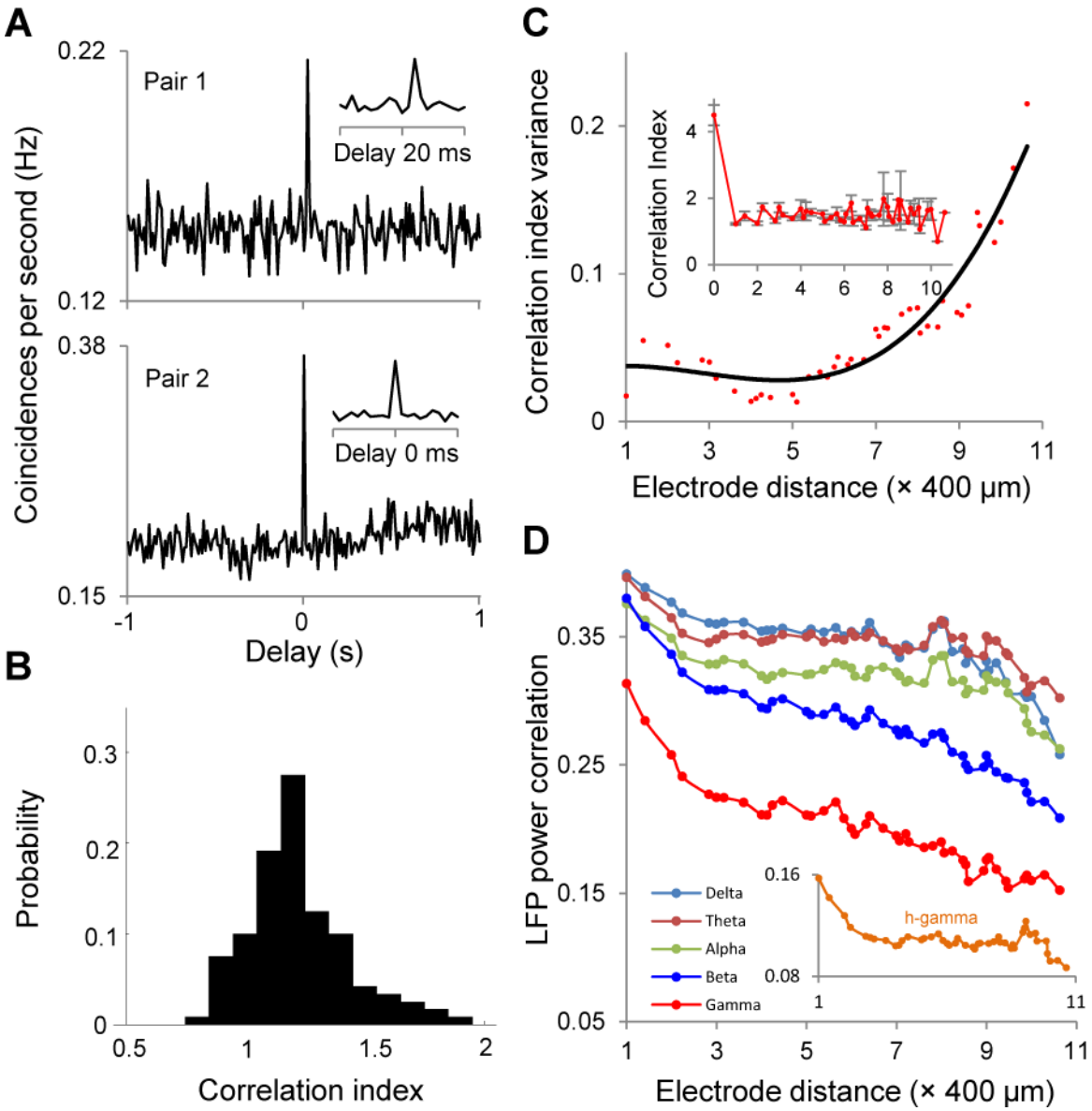

Figure 5.

Wireless monitoring of population activity during free exploration. Measure the cross-correlation between pairs of dlPFC neurons recorded from the same or different channels while the monkey was freely moving in its cage. (A) Most pairs (73.7%) showed peaks near zero lag (bottom) to indicate synchronized firing pairs. Correlation peaks displaced from the zero lag were observed less often (top). (B) Across all the recorded pairs, the correlation index was biased to positive values. (C) Correlation index as a function of the distance between the dlPFC neurons. Plots indicating a peak in the correlation index between dlPFC cell pairs from the same electrode, and a sharp decline in the mean correlation index between neurons separated by 400 μm or more (inset). (D) Correlations in LFP power by computing the Pearson correlation of band-limited LFP power between two electrodes as a function of electrode distance (in the 400–4400μm range). The LFP correlations decrease as a function of electrode distance (see main text).

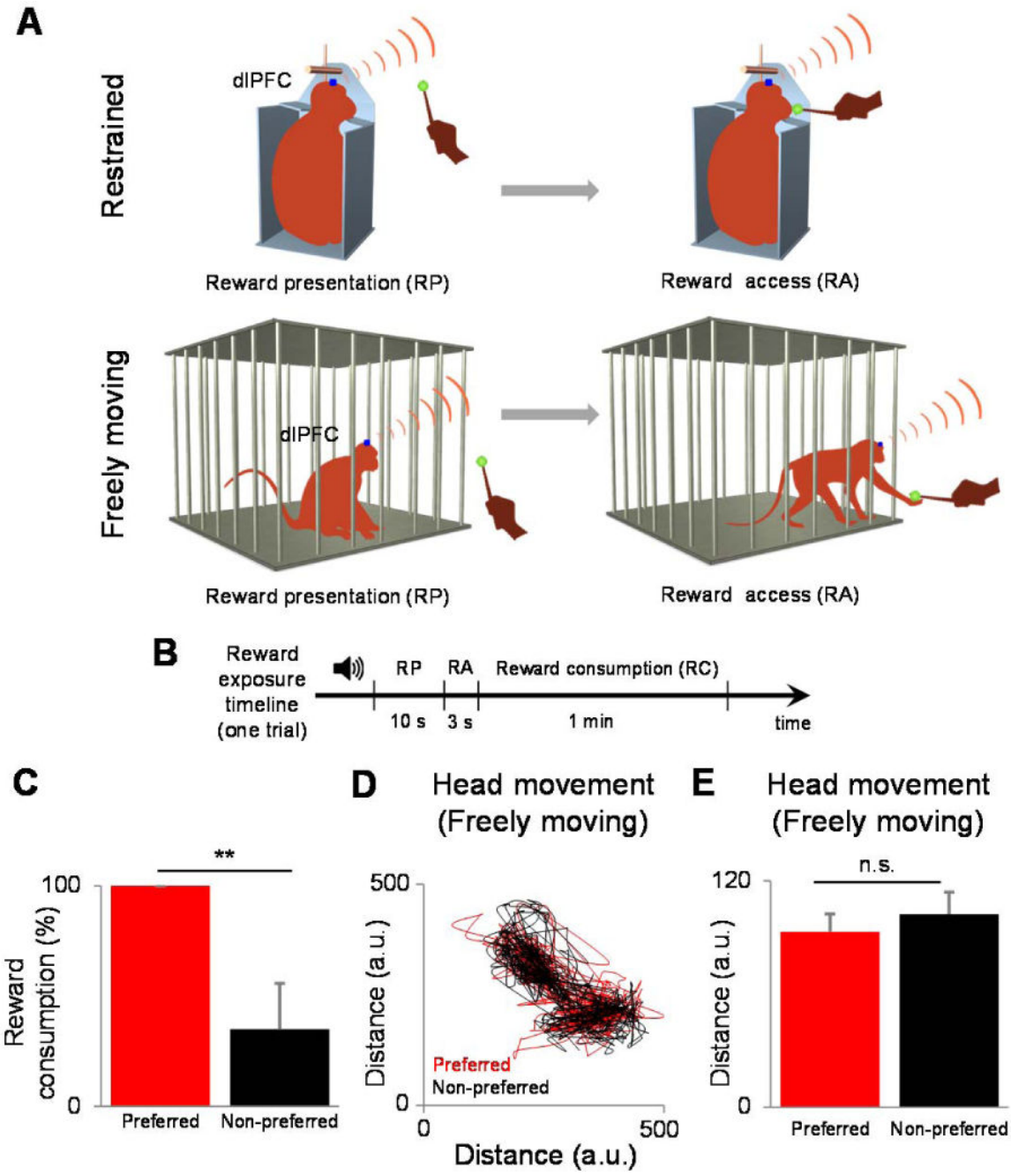

Figure 6.

Experiments examining changes in dlPFC responses in two conditions: (A) head-fixed and movement-restrained condition (top) and when the animal freely roamed in its cage (bottom). (B) The monkey performed 24 trials per reward type per session (five restrained and five freely moving sessions), and each reward type represented one trial. (C) Plot showing that as expected, the animal consumed the preferred reward more often than the non-preferred reward. (D) We quantified the movement of the animal by video recording the movements of the monkey in the freely moving condition then tracking the movements of the monkey's head of offline by using the transmitter as the reference point (see section 4).

(E) We did not observe a significant difference between the extent of movement associated with the preferred and non-preferred reward types during the reward presentation

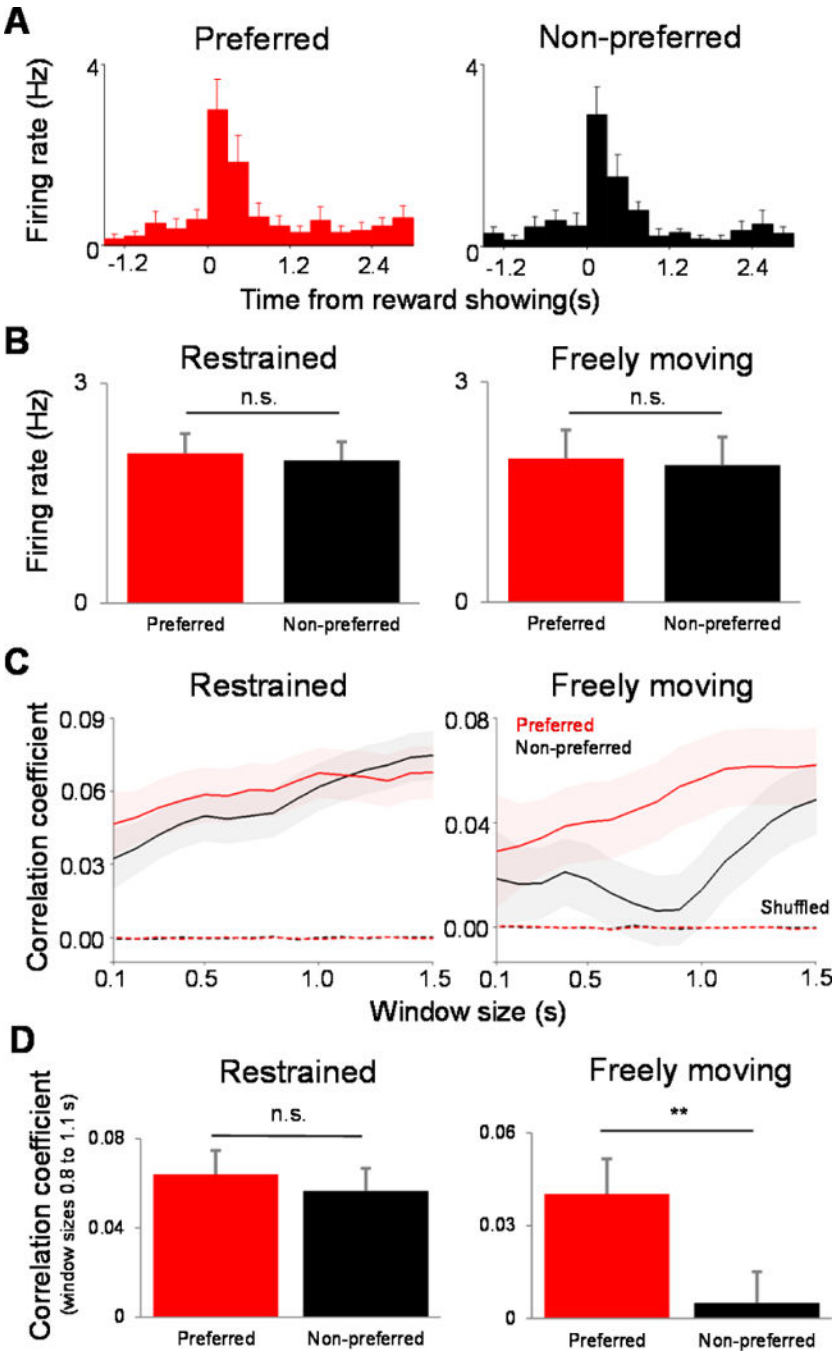

Figure 7.

Reward-dependent changes in neuronal correlations in the unrestrained condition. (A) Plots showing firing-rate histograms for one example neuron responding to both types of reward. (B) Results indicating that the population average firing rates for the two reward types (1000 ms following stimulus onset) were not significantly different from each other during the restrained and freely moving condition, and similar results were obtained when we extended the size of the window in which spikes were counted for the entire 10 s interval when the stimulus was presented. (C) Pearson correlation values associated with the two reward types

as a function of expanding window size, starting from the time when the reward was first presented (see main text). (D) The mean correlation coefficient associated with the two types of reward was significantly different from each other (right). However, when the monkey was restrained, neuronal correlations associated with the preferred and non-preferred rewards were not statistically different (left).